Aalborg Universitet

AALBORG UNIVERSITY

Seamless Transition of Microgrids Operation from Grid-Connected to Islanded Mode

Ganjian-Aboukheili, M.; Shahabi, M.; Shafiee, Q.; Guerrero, Josep M.

Publication date:
2020

Document Version
Accepted author manuscript, peer reviewed version

Link to publication from Aalborg University

Seamless Transition of Microgrids Operation from Grid-Connected to Islanded Mode

M. Ganjian-Aboukheili, M. Shahabi, *Member, IEEE*, Q. Shafiee, *Senior Member, IEEE*, and Josep M. Guerrero, *Fellow, IEEE*

Abstract-- **One of the main features of Microgrids is the ability to operate in both grid-connected mode and islanding mode. In each mode of operation, distributed energy resources (DERs) can be operated under grid-forming or grid-following control strategies. In grid-connected mode, DERs usually work under grid-following control strategy, while at least one of the DERs must operate in grid-forming strategy in islanding mode. A microgrid may experience remarkable fluctuations in voltage and current due to an unintentional islanding event. To achieve a smooth transition to islanding mode and mitigate disturbance effect, this paper proposes a control strategy includes a) a linear voltage controller with capacitor current feedback as an input to the voltage controller and output current feedforward as an input to current controller, and b) modified droop control to emulate the inertia response of a synchronous generator. The proposed controller can suppress voltage, current and frequency fluctuations and also guarantee a smooth transition. A small signal analysis of the proposed control strategy is developed to design its coefficients as well as the destabilizing effect of constant power load (CPL). Experimental results are provided to verify the effectiveness of the proposed control strategy.**

Index Terms— **Grid-connected, islanding mode, microgrids, modified droop control, smooth transition.**

I. INTRODUCTION

MICROGRID, as a small-scale power system, can work in both grid connected (GC) and islanding (IS) modes. In each mode of operation, distributed energy resources (DER) in microgrids (MGs) can be controlled using different strategies. DERs based on power electronic converters are usually the dominant part of a MG. DERs can operate in two different modes, 1) current source with grid-following control strategy and 2) voltage source with grid-forming control strategy [1]. The former is useful for converters that only inject a specific current to the MG e.g., converter used for the renewable energy source (RES), while the latter can be employed in both modes of operation. In GC mode, the voltage and frequency of the MG are dictated by upstream grid, thus DERs tend to operate in grid-following strategy. In islanding mode, however, it is crucial to have some of DERs operating in grid-forming strategy to regulate the voltage and frequency of the MG.

The stability and robustness of a MG depends on the performance of the DERs. Number of control strategies have been introduced for DERs in the literature which can be used in both GC and IS modes of operation [2]. These control strategies can be categorized into two types [3]: 1) control strategies for both modes of operation with a single control scheme (usually based on voltage control) which remain in service to provide further capabilities [4]-[9], 2) control strategies with two different control schemes where each mode is activated according to the pre-assigned control objective [10]-[15].

The majority of the first types of controllers are based on nonlinear control theory, e.g., Lyapunov-based method [5], [8], model predictive control [4], [9], which usually need an accurate model of the system and DER dynamic behavior. However, these controllers not only have a complex structure with a high computational burden but also their realization is very difficult. Furthermore, these types of control techniques are not easily implementable in practice. In contrary, linear control strategies provide a simple structure, low computational burden, and they are very convenient in design and implementation [9]. Due to using feedback or feedforward of the physical variables, linear control strategies give a better sense to the controller performance. Cascade control strategies have already been introduced in control design and implementation [16], [17].

These types of controllers must be able to not only operate in both modes of operation, but also provide a seamless transition between them. This transition should occur smoothly while eliminating the disturbances or at least staying within a reasonable limit. During transition, the following issues may exist: 1) frequency fluctuation because of transition from a grid-following to a grid-forming strategy which leads to a disturbance on the power-angle of DERs and even threats the MG stability, 2) voltage and current deviation in DERs output due to switching between the modes.

In the MGs, the transition occurs in two cases: a) IS mode to GC and b) GC to IS mode. The former case corresponds to the synchronization procedure where the voltage at the point of common coupling (PCC) must follow the main grid. According to the synchronizing criteria described in IEEE.std.1547-2003, ±10% in voltage amplitude difference, 0.3 Hz for frequency difference, and 20 degrees for phase difference are standard ranges [18]. Therefore, by utilizing a proper synchronization

algorithm, the transition may be smooth and no disturbance will be imposed on the MG. The latter case (i.e., transition from GC to IS mode) could happen either intentional or unintentional. In the intentional islanding, transition intensity can be controlled by means of re-adjusting the MG operation point. The unintentional islanding, which is the main focus of this paper, occurs suddenly and re-adjusting the operation point of DERs is not a feasible solution. Hence, the frequency and voltage amplitude of the MG will be suffered by large disturbances and may endanger the system stability.

Various techniques have been introduced in the literature which aims to minimize the effects of disturbances during a transition process [5], [6], [9], [10], [12], [19]. In [6] and [18], droop-based control strategies are introduced where no switching is needed between controllers used in both modes. Alternatively, nonlinear control strategies have been introduced [5], [9], [10] and [19]. Authors in [5] proposed a nonlinear control strategy using an adaptive back-stepping technique to operate in both modes of operation. A nonlinear control based on a variable structure is investigated in [10] to mitigate large disturbances such as islanding transition. A model predictive control is proposed in [9] which is applied on a single phase inverter to operate in both modes. This MPC framework uses a hybrid objective function with auto-tuning weighting factors. Seamless transition between modes of operation has been mostly investigated for MGs with a single DER, while in practice, MGs consist of multi DERs with multi buses. Hence, it is important to investigate the interaction between controllers of different DERs in this situation. This interaction is usually associated with power angle swing defined by power sharing between DERs during the transition. During transition to islanding mode, the power angle and frequency may be imposed by large swings. To have a smooth transition, the damping ratio needs to be improved. To reduce frequency deviation during MG transition, virtual inertia can be a good solution [20].Virtual synchronous generator (VSG) and droop control are two methods to implement virtual inertia [21]. Although, small-signal model of the VSG control is equivalent to droop control in some cases, their dynamic performance don't exactly be same [20]. In [20], it was shown VSG has larger inertia than droop control. However, output active power of VSG is more oscillatory than droop control. The oscillations may be amplified when the governor delay is added to VSG control. Due to more popularity of droop control utilization in microgrid application, this method can have the potential to contribute inertia response during transition mode as well as VSG. If the parameters in the droop control is designed properly according to the system requirements, the dynamic performance of the inverter can be even better than VSGs [22]. Although, in [6] and [16], a derivative term is added to droop mechanism for power sharing improvement, to involve the virtual inertia into droop control, a modified droop control is required to propose.

Aiming to achieve a smooth transition from GC to IS mode, proper load sharing between DERs and also enhancing system stability, this paper proposes a control strategy by modifying conventional droop control and voltage control. Opposed to the high complexity of nonlinear strategies or unreliable operation of linear strategies under abnormalities, the main contributions of this paper can be summarized as follows:

1) A modified linear voltage control strategy with an output current feed-forward and capacitor current feedback gained by high pass filter is proposed which are added to the voltage loop and current loop, respectively. This strategy can improve system dynamic performance by providing more damping, mitigate disturbances effects, and compensate transient voltage drop at inverter output. Because of linear structure, it is convenient for engineering implementation.

2) A modified droop mechanism is constructed to adjust its coefficient according to active power variation. This technique which is inspired by inertia response of synchronous generator could enforce undesirable frequency over/undershoot in disturbances.

3) In order to insightfully study the performance of the proposed strategy, a stability analysis is investigated through the small signal model of the test MG with various loads.

The effectiveness of the proposed control strategy is validated by theoretical analysis and experimental results. The rest of this paper is organized as follows. Section II describes the MG configuration and different operation modes. A control strategy for a seamless transition with a smooth response is proposed in section III, and the small signal analysis is done in section IV. Experimental results are represented in section V. Section VI concludes the paper.

II. MICROGRID CONFIGURATION AND CONTROL STRUCTURE

Fig. 1 shows the general scheme of a MG with three converter-based DERs. It is assumed that the dynamic behavior of the DERs' prime movers is neglected, represented by a dc voltage source (Vdc).
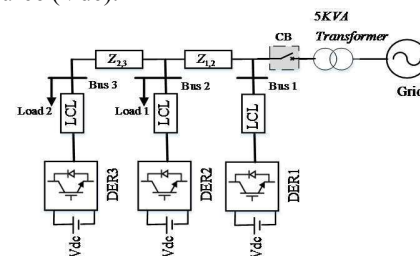

Fig. 1. Schematic of a MG including three converter-based DER.

For each DER, a three-phase inverter equipped with an LCL filter is connected to the bus. The MG is connected to the grid through a circuit breaker (CB) placed in PCC. It should be noted that DERs controller doesn't have any control over CB and thus the CB status is unknown. The MG is connected to the upstream grid at PCC (Bus1) through a 5kVA power transformer. The circuit breaker will be opened consequent to a disturbance such as a fault event in the upstream grid. All DERs in the test system are voltage source inverters (VSIs).

The overall control structure of a converter-based DER is shown in Fig. 2, where DER can be operated in either grid-forming (VCM) or grid-feeding control strategy (CCM). Once a mode transfer command is received, the controller switches to another mode of operation.
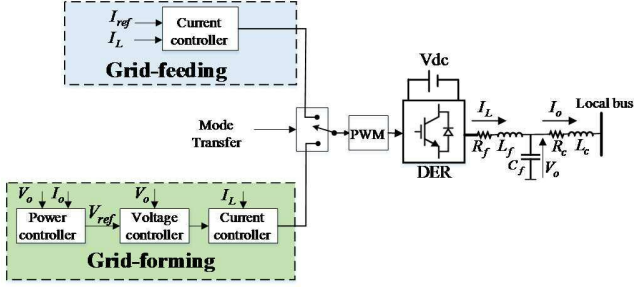
Fig. 2. Overall structure of the conventional control strategy for a converter-based DER with GC and islanded mode operation capability.

A. Grid Connected Mode

In GC mode, DERs usually operate under grid-feeding strategy or CCM. The conventional current control structure is based on PI [23] or PR [24] controller which are implemented in the dq or $\alpha\beta$ reference framework, respectively. Fig. 3 shows the current control loop block diagram considering PWM delay and physical filter (LC) in the dq reference framework.

With the decoupling approach, the model can approximately be simplified into two identical SISO systems. Hence, the subscript d and q are ignored in the following analysis. The closed-loop transfer function of the system (control part and physical plant) is derived as follows [23]:

$$I_L = \frac{G_i(s)G_{pwm}(s)C_f s}{L_f C_f s^2 + R_f C_f s + G_i(s)G_{pwm}(s)C_f s + 1 - G_{pwm}(s)} I_{ref}$$
$$- \frac{G_{pwm}(s)-1}{L_f C_f s^2 + R_f C_f s + G_i(s)G_{pwm}(s)C_f s + 1 - G_{pwm}(s)} I_o \quad (1)$$

where L_f, C_f and R_f are the LC filter parameters, I_{ref} is the current reference, $G_{PWM}(s)$ is the PWM delay transfer function, and $G_i(s)$ is a simple PI controller [15], [25].
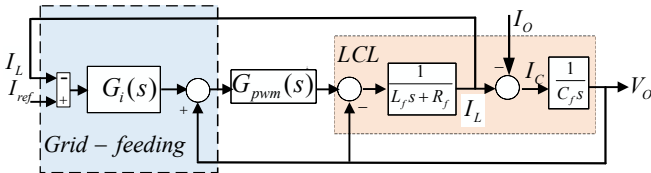

Fig. 3. Block diagram of the conventional current control structure.

Using (1) and applying KCL in capacitor node of the LC filter, the equivalent circuit of inverter in CCM can be derived as:

$$I_o = \underbrace{G_c(s)I_{ref}}_{I_{DER}} - Y_o V_o \quad (2)$$

which is a representation of the Norton equivalent circuit. Thus, DER can be modeled by an equivalent circuit in this operation mode as shown in Fig. 4(a) [26].
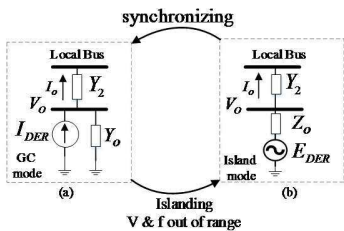

Fig. 4. DER equivalent circuit in both (a) grid-feeding control strategy and

(b) grid-forming control strategy.

The equivalent circuit is represented by a constant current source in parallel with an admittance Y_o. Y_2 is the line admittance between the inverter output and its local bus.

B. Islanding Mode

The grid-forming control strategy is commonly based on the cascade loops [16] and [17] including power controller, voltage controller, and current controller. The power controller is a conventional droop control which provides voltage amplitude and phase references of inner loops. The conventional droop mechanism can be expressed as follows:

$$\omega = \omega^* - m(P - P^*), \qquad E = E^* - n(Q - Q^*) \quad (3)$$

where ω, E, ω^* and E^* are angular frequency and output voltage amplitude of the inverter, reference angular frequency and voltage amplitude, respectively. P and Q are the measured active and reactive power output passed through a low pass filter with a small cut-off frequency (w_c), P^* and Q^* are active and reactive power references. m and n are droop coefficients. The block diagram of the conventional VCM is shown in Fig. 5. The closed-loop transfer function for the conventional VCM is expressed in (4).
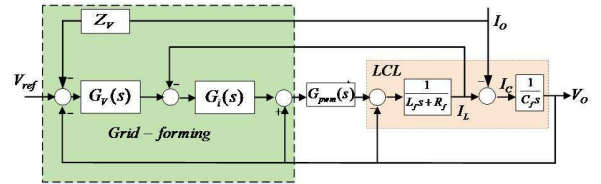

Fig. 5. Block diagram of conventional VCM with output voltage and inductor current feedback and virtual impedance.

$$V_o = \frac{G_v(s)G_i(s)G_{pwm}(s)}{L_f C_f s^2 + R_f C_f s + G_i(s)G_{pwm}(s)(G_v(s)+C_f s) + 1 - G_{pwm}(s)} V_{ref}$$
$$- \frac{L_f s + R_f + G_i(s)G_{pwm}(s)(G_v(s)Z_v(s)+1)}{L_f C_f s^2 + R_f C_f s + G_i(s)G_{pwm}(s)(G_v(s)+C_f s) + 1 - G_{pwm}(s)} I_o \quad (4)$$

where $G_v(s)$ is the voltage controller transfer function and V_{ref} is the reference voltage. The output voltage (4) can be described by $G_{conv}(s)$ is the closed-loop transfer function of the conventional VCM strategy.

$$V_o = \underbrace{G_{conv}(s)V_{ref}}_{E_{DER}} - Z_o^{conv} I_o \quad (5)$$

$$\begin{cases} G_{conv}(s) = \\ \dfrac{G_v(s)G_i(s)G_{pwm}(s)}{L_f C_f s^2 + R_f C_f s + G_i(s)G_{pwm}(s)(G_v(s)+C_f s) + 1 - G_{pwm}(s)} \\ Z_o^{conv}(s) = \\ \dfrac{L_f s + R_f + G_i(s)G_{pwm}(s)(G_v(s)Z_v(s)+1)}{L_f C_f s^2 + R_f C_f s + G_i(s)G_{pwm}(s)(G_v(s)+C_f s) + 1 - G_{pwm}(s)} \end{cases} \quad (6)$$

The output impedance Z_o^{conv} can be reshaped through a virtual impedance (Z_v) for different objectives such as power sharing [27]. According to (5), the DER can be modeled by a Thevenin equivalent circuit. Fig. 4(b) shows the equivalent circuit of the DER in grid-forming strategy which is represented by a voltage source in series with an impedance Z_o.

This article has been accepted for publication in a future issue of this journal, but has not been fully edited. Content may change prior to final publication. Citation information: DOI 10.1109/TSG.2019.2947651, IEEE Transactions on Smart Grid

4

C. Transition Between Modes

In opposed to intentional islanding, it is impossible to adjust DER controller set-point or its operation point instantaneously in the case of unintentional islanding. In such a case, voltage and current output of DER may experience large deviation because of the low inertia of power electronic converters. The performance of the DER controller is the most effective factor on fluctuations' magnitude and its duration in transition mode. Therefore, the controller in islanding mode must be able to resist against large deviations and maintain the steady state condition within an accepted range.

Fig. 6 shows the transition procedure of a MG from grid-connected to islanding mode. It is assumed that the MG operates in the grid-connected mode. At $t=T_1$, the circuit breaker is opened consequent to unintentional islanding. Islanding detection algorithm confirms the islanding situation in a few power cycles. At $t=T_2$, the mode transfer signal (switch to the grid-forming strategy) is issued. Thus, DERs continue to operate in grid feeding strategy within the time interval T_1 to T_2.
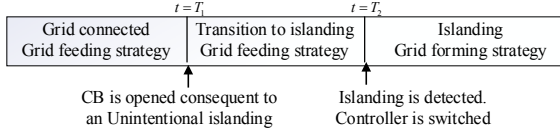

Fig. 6. The time procedure of an unintentional islanding.

III. PROPOSED CONTROL STRATEGY

In this section, the objective is to propose a control strategy for DERs at the primary level in order to have a good performance in the transition from GC to IS mode consequent upon unintentional islanding. Fig. 7 shows the structure of the proposed control strategy for a converter-based DER. A smooth transition compensator is added to the control structure of Fig. 2 to guarantee fluctuations mitigation.
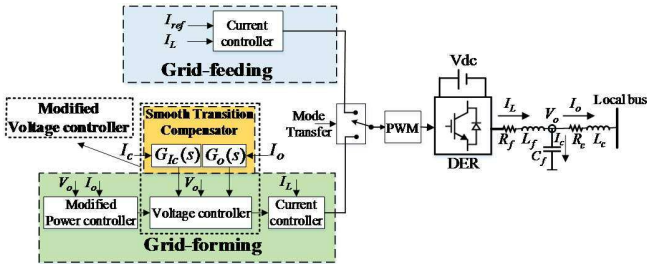

Fig. 7. Overall structure of the proposed control strategy for a converter-based DER.

The compensator has two inputs including capacitor current (I_c) and output current (I_o). The appropriate output signals are generated by two different transfer functions, and then added to the voltage controller. The voltage controller with smooth transition compensator called as a modified voltage controller.

A. Modified Voltage Controller

The magnitude and duration of the deviations depend on performance of the controller. In order to enforce the magnitude and duration of the deviations in an acceptable limit, the voltage controller must provide more damping. By adding the capacitor current feedback to the voltage loop in Fig. 2, the new voltage

references can be calculated as:

$$V_{ref}^* = V_{ref} - G_{Ic}(s)I_c \qquad (7)$$

where I_c is the capacitor current and $G_{Ic}(s)$ is a high pass filter. $G_{Ic}(s)$ is expressed as:

$$G_{Ic}(s) = \frac{K_{Ic}s}{s + w_{Ic}} \qquad (8)$$

K_{Ic} and w_{Ic} are gain and cut-off frequency.

Using this feedback, the VCM strategy in Fig. 5 is modified as Fig. 8. By combining (7) and (5), the closed-loop transfer function of the output voltage ($V_o - V_{ref}$) is

$$V_o = G_{conv}(s)V_{ref}^* = G_{conv}(s)(V_{ref} - G_{Ic}(s)I_c) \qquad (9)$$

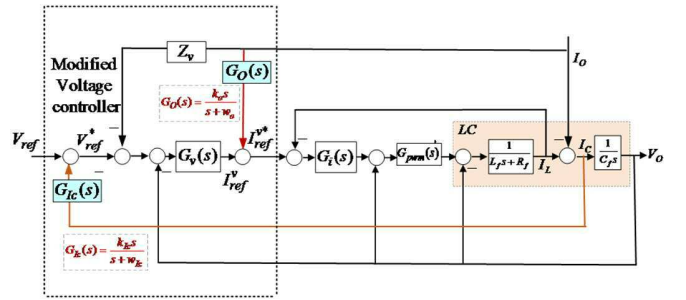Using $I_c = C_f s V_o$ one can write:

Fig. 8. Block diagram of the proposed control strategy with modified voltage controller in islanding mode.

$$V_o = G_{conv}(s)(V_{ref} - G_{Ic}(s)C_f s V_o) \qquad (10)$$

Thus, the final form of the closed loop transfer function is obtained as:

$$V_o = \frac{G_{conv}(s)}{1 + G_{conv}(s)G_{Ic}(s)C_f s}V_{ref} = G_{proposed}(s)V_{ref} \qquad (11)$$

To analyze the performance of the proposed controller, time domain (step response) and frequency domain (frequency response) studies are done. The MG and controller parameters are given in Table I. The comparative results of the frequency response of the closed-loop tracking voltage transfer function $G_{proposed}(s)$ and $G_{conv}(s)$ are shown in Fig. 9. It can be found that the proposed controller mitigates the peak magnitude in the frequency response. It is clear that the bandwidth of the conventional controller is lower than the proposed controller.
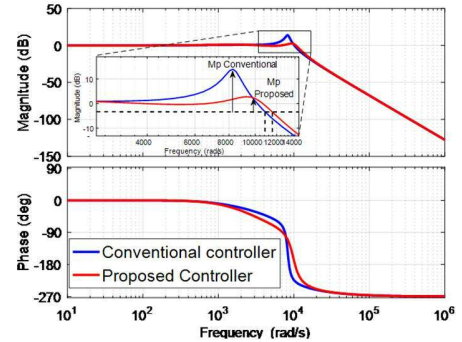

Fig. 9. Frequency response of the closed-loop transfer function (V_o-V_{ref}) of $G_{conv}(s)$ and $G_{proposed}(s)$ with K_{Ic}=15 and w_{Ic}=400Hz.

To verify the effectiveness of the proposed controller $G_{proposed}(s)$ compared to $G_{conv}(s)$, their step responses are depicted in Fig. 10.
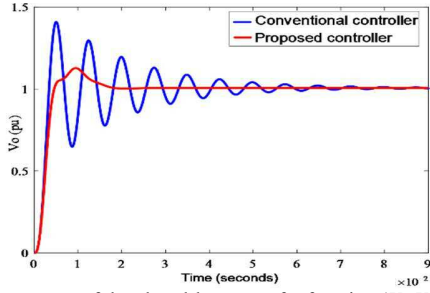
Fig. 10. Step response of the closed-loop transfer function (V_o-V_{ref}) of $G_{conv}(s)$ and $G_{proposed}(s)$ with K_{Ic}=15 and w_{Ic}=400Hz.

According to Fig. 5, the output current (I_o) can be modeled as a disturbance in the simplified block diagram of the control strategy with LC filter plant. The output voltage is known to have a relation with output current as (5). Thus, a fluctuation in the output current could affect the output voltage directly.

In order to decrease output current disturbance effect on the output voltage, a feed-forward of the output current is added to the proposed voltage control strategy as an input of the current controller (see Fig. 8). Thus, new reference of the current controller is obtained as:

$$I_{ref}^{v*} = I_{ref}^{v} + G_o(s)I_o \tag{12}$$

where I_{ref}^{v*} and $G_o(s)$ are new current reference and high pass filter transfer function, respectively. $G_o(s)$ can be described as:

$$G_o(s) = \frac{K_o s}{s + w_o} \tag{13}$$

where K_o and w_o are gain and cut-off frequency.

By applying feed-forward current, the closed-loop transfer function ($V_o - I_o$) in (6) is modified as:

$$Z_o = Z_o^{conv} - G_i(s)G_{pwm}(s)G_o(s) \tag{14}$$

By considering the capacitor current feedback in Fig. 8, the equivalent output impedance for the proposed control strategy can be expressed as follows:

$$Z_o^{proposed} =$$

$$\frac{L_f s + R_f + G_i(s)G_{pwm}(s)(1+G_v(s)Z_v - G_o(s))}{L_f C_f s^2 + R_f C_f s + G_i(s)G_{pwm}(s)(G_v(s)+G_v(s)G_{Ic}(s)C_f s + C_f s)+1-G_{pwm}(s)} \tag{15}$$

Frequency and step response of the proposed and conventional approaches, for the output impedance, are sketched in Fig. 11 and Fig. 12, respectively.
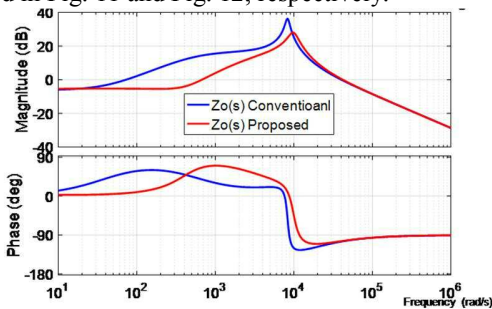

Fig. 11. Frequency response of the closed loop transfer function of (V_o-I_o) for conventional (Z_o^{conv}) and proposed controller ($Z_o^{proposed}$).
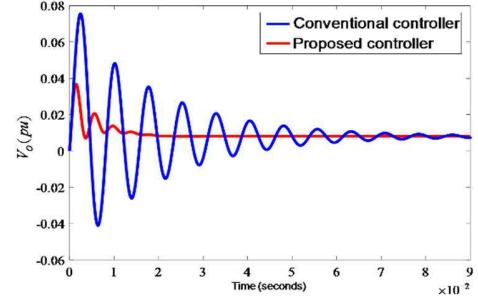

Fig. 12. Step response of the closed loop transfer function of (V_o-I_o) for conventional (Z_o^{conv}) and proposed controller ($Z_o^{proposed}$).

The proposed approach has a smaller peak in resonance frequency and higher bandwidth than the conventional approach. It can be seen the proposed approach has a smaller gain in a wide range of frequency, which means large disturbance rejection. Moreover, the overshoot magnitude and oscillations are decreased significantly in the proposed approach (see Fig. 12).

Finally, according to Fig. 8, the closed-loop transfer function of the modified voltage controller can be expressed as:

$$\begin{cases} G_{proposed}(s) = \dfrac{G_v(s)G_i(s)G_{pwm}(s)}{\Delta} \\ Z_o^{proposed} = \dfrac{L_f s + R_f + G_i(s)G_{pwm}(s)(1+G_v(s)Z_v - G_o(s))}{\Delta} \end{cases}$$

$$\Delta = L_f C_f s^2 + R_f C_f s + G_i(s)G_{pwm}(s)(G_v(s)+G_v(s)G_{Ic}(s)C_f s + C_f s)+1-G_{pwm}(s) \tag{16}$$

B. Modified Droop Control

As mentioned above, the output voltage phase changing or jumping at switching time between two controllers will increase the output voltage and current deviations. As shown in Fig. 9, the closed loop transfer function (16) of inner loops (current controller and voltage controller) has a unity gain and zero phase shift in a wide range of frequencies. Thus, the output voltage phase and amplitude of the DER can approximately be determined by power controller which is based on droop mechanism in this work. The output voltage reference generated by droop control can be expressed as [16]:

$$V_{ref} = E\sin(\omega^* t + \varphi) \tag{17}$$

where E is the voltage amplitude reference, ω^* is the angular frequency reference, and φ is the generated phase by (5).

Although the conventional droop provides some advantages, the deviation of phase associated with mode transition or load switching in islanding mode, may affect the MG stability. To deal with this issue, the conventional frequency droop mechanism can be rearranged as follows:

$$P - P^* = \frac{1}{m}(\omega - \omega^*) + T_{wc}\frac{1}{m}s\omega \tag{18}$$

where T_{wc} is the time constant of low pass filter in droop control, and T_{wc}/m and $1/m$ are the equivalent moment of inertia and damping coefficient, respectively. Therefore, the system inertia would increase by decreasing m which could enforce phase deviation at a low level. Thus, a modified droop

control is proposed to adjust its coefficient properly. The general form of the modified droop control is given as follows:

$$\omega = \omega^* - f_i(m, P, \frac{dP}{dt}) \qquad (19)$$

One can write the function $f_i(.)$ of (19) as

$$f_i(m, P, \frac{dP}{dt}) = \underbrace{me^{-\beta|\frac{dP}{dt}|}P}_{\text{Proposed nonlinear term}} - \underbrace{m_d \frac{dP}{dt}}_{\text{Derivative term}} \qquad (20)$$

the $Q - E$ droop equation is introduced as follows:

$$E = E^* - nQ - n_d \frac{dQ}{dt} \qquad (21)$$

where m_d, n_d and β are the derivative coefficients and exponential coefficient respectively. The performance and stability of the derivative term is studied in [8] and [16]. In steady state dp/dt will be equal to zero and the proposed droop control behaves like the conventional droop. A dead-band is employed for dp/dt to avoid enabling against minor variations.

IV. SMALL SIGNAL ANALYSIS

The proposed control strategy parameters must be designed in such a way that the MG stability is guaranteed. According to Fig. 9 to Fig. 12, inner loops have a desirable behaviors. It is noticeable that the power controller is the lowest control loop and it could be analyzed separately ignoring inner loops dynamic behavior [16], [26]. Hence, for stability evaluating of the modified droop control, a small signal analysis has been conducted. Power injection of a DER connected to the grid through a reactance can be expressed [16] as follow:

$$P = \frac{EV}{X} \sin\varphi \qquad (22)$$

$$Q = \frac{EV}{X} \cos\varphi - \frac{V^2}{X} \qquad (23)$$

By linearizing (22) and (23) around a specific operation point, one can write:

$$\begin{bmatrix} \Delta P \\ \Delta Q \end{bmatrix} = \frac{w_c}{s+w_c} \frac{V}{X} \begin{bmatrix} \sin\Phi & E\cos\Phi \\ \cos\Phi & -E\sin\Phi \end{bmatrix} \begin{bmatrix} \Delta E \\ \Delta\varphi \end{bmatrix} \qquad (24)$$

where ΔP, ΔQ, ΔE, and $\Delta\varphi$ are small perturb around operation point. E, Φ and V are operation point variables and X is output reactance. The Linear model of the proposed droop control with the assumption of $e^\alpha \approx (1 + \alpha)$ is derived as:

$$\omega = \omega^* - m(1-\beta\frac{dP}{dt})P - m_d\frac{dP}{dt} \qquad (25)$$

By perturbing above equation around the equilibrium point and assuming $(\Delta P)^2 \approx 0$, Laplace form of (25) and (21) are obtained as:

$$\Delta\omega = \Delta\omega^* + (-m + \beta mP_0 s - m_d s)\Delta P \qquad (26)$$

$$\Delta E = \Delta E^* - n\Delta Q - n_d s\Delta Q \qquad (27)$$

By using (24), (26) and (27), the small signal model becomes:

$$s\Delta\varphi = \Delta\omega = (-m + \beta mP_0 s - m_d s)$$
$$\times \frac{w_c}{w_c + s} \frac{V}{X} [\sin\Phi\Delta E + E\cos\Phi\Delta\varphi] \qquad (28)$$

$$\Delta E = -(n + n_d s)\frac{w_c}{w_c + s} \frac{V}{X} [\cos\Phi\Delta E - E\sin\Phi\Delta\varphi] \qquad (29)$$

By substituting (29) into (28), one can write

$$s\Delta\varphi = (-m + m\beta P_0 s - m_d s)\times$$
$$\frac{w_c}{w_c + s} \frac{V}{X} \left[\frac{(n + n_d s)w_c \frac{V}{X}E\sin\Phi}{(w_c + s + w_c(n + n_d s)\frac{V}{X}\cos\Phi)}\Delta\varphi + E\cos\Phi\Delta\varphi \right] \qquad (30)$$

Finally, the characteristic equation is calculated as:

$$s^3 + As^2 + Bs + C = 0 \qquad (31)$$

$$A = \frac{w_c}{X_d}[2X + nV\cos\Phi + n_d w_c V\cos\Phi + m_d EV(w_c n_d \frac{V}{X} + \cos\Phi)$$
$$+ VE\beta mP_0(w_c n_d \frac{V}{X} + \cos\Phi)] \qquad (32)$$

$$B = \frac{w_c}{X_d}[Xw_c + nw_c\frac{V}{X}\cos\Phi + mEV\cos\Phi + mn_d w_c\frac{V}{X}\cdots$$
$$+ m_d EV w_c(n\frac{V}{X} + \cos\Phi) + VE\beta mP_0 w_c(n\frac{V}{X} + \cos\Phi)] \qquad (33)$$

$$C = w_c^2\frac{V}{X_d}mE(n\frac{V}{X} + \cos\Phi) \qquad (34)$$

where $X_d \triangleq X + n_d w_c V\cos\Phi$. By using the characteristic equation and the parameters displayed in Table I, the root locus is provided in Fig.13. Fig. 13(a) shows the root locus of the system for different values of m and β. It can be seen that complex eigenvalues (λ_2, λ_3) move toward real axis with the larger real part when β is increased. It means that the system would have more damping. The root locus of the system for different values of m_d and β is illustrated in Fig. 13(b). With increasing m_d and β, complex eigenvalues are adopted larger real part and smaller imaginary part so that we can obtain improved dynamic performance of the system.
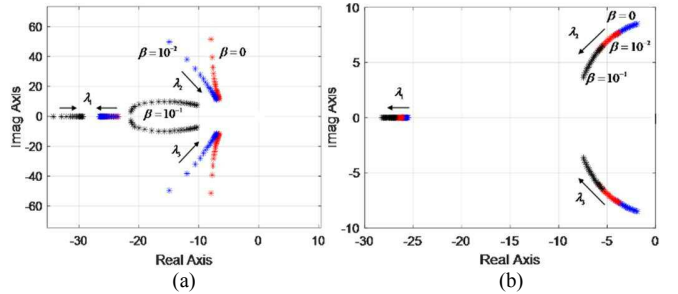

Fig. 13. Root loci of the system considering the proposed solution: (a) $\beta = 0, 10^{-2}$ and 10^{-1} and $m_d = 7 \times 10^{-7}$ for $10^{-6} \le m \le 32 \times 10^{-5}$, (b) $\beta = 0, 10^{-2}$ and 10^{-1} and $m = 32 \times 10^{-5}$ for $10^{-7} \le m_d \le 10^{-6}$.

It is worth mentioning that dynamic loads such as motors influence the system dynamics. These dynamics can be modeled as a CPL in small signal stability analysis [28]. The complete small signal model of the MG with loads can be found in [29]. To evaluate efficacy of the proposed controller under dynamic loads, the small signal model of the test MG have been developed. The complete small signal model of the test MG can be described as follows:

$$\begin{bmatrix} \Delta\dot{x}_{INV} \\ \Delta\dot{i}_{lineDQ} \\ \Delta\dot{i}_{loadDQ} \end{bmatrix} = A_{MG}\begin{bmatrix} \Delta x_{INV} \\ \Delta i_{lineDQ} \\ \Delta i_{loadDQ} \end{bmatrix} \qquad 35)$$

Model Matrices can be found in [29] which are calculated based on the given parameters in Table. I. The dominant

This article has been accepted for publication in a future issue of this journal, but has not been fully edited. Content may change prior to final publication. Citation information: DOI 10.1109/TSG.2019.2947651, IEEE Transactions on Smart Grid

7

eigenvalues of the derived model are illustrated in Fig. 14.

According to Fig. 14 (a), the system has eigenvalues with positive real part in conventional strategy. These positive eigenvalues are increasing with negative incremental resistance increasing of CPL. In order to overcome destabilizing effect of CPL, the proposed strategy can change positive eigenvalues toward left half plane which is shown in Fig. 14 (b).
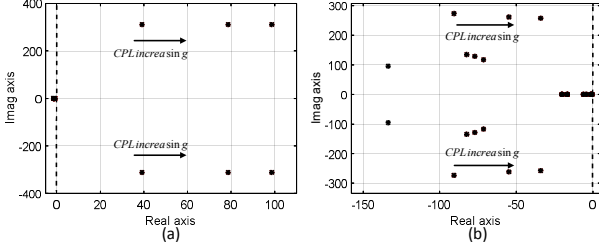

Fig. 14. Root loci of the dominant eigenvalues of the system considering dynamic loads: (a) conventional strategy, (b) the proposed strategy.

V. EXPERIMENTAL RESULTS

The MG system, shown in Fig. 1, was implemented in the Intelligent MG Laboratory at Aalborg University to evaluate the performance of the proposed approach. Fig. 15 shows a photo of the experimental setup. Three 2.2 kW Danfoss inverters equipped by LCL filters and line and load impedances were used to build the MG setup. A power transformer is used as grid and a controllable switch to emulate CB. The proposed approach is first constructed in MATLAB/Simulink and then implemented in an HIL-based real-time simulation platform (dSPACE1006). The electrical and control parameters are given in Table I.
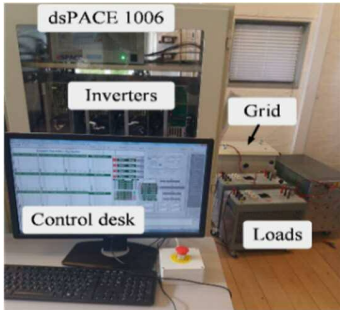

Fig. 15. Experimental setup for implementing the MG system in Fig. 1.

TABLE I
ELECTRICAL AND CONTROL PARAMETERS

Parameters	Symbol	Value
MG voltage (peak magnitude)	V_{nom}	325 V
Switching frequency	f_s	10 kHz
Filter inductance LCL	L_f, L_C	1.8 mH
Filter capacitance LCL	C_f	25 µF
Virtual Impedance	R_V, L_V	0.5Ω, 3.6 mH
Line impedance 1,2	$Z_{1,2}$ $Z_{2,3}$	0.8 Ω, 3.6 mH 0.4 Ω, 1.8 mH
Load at bus 2,3	L_1 L_2	150 Ω, 0.1 H 300 Ω, 0.3 H
Droop coefficient P-W	m	0.00032 rad/s.W
Droop coefficient Q-V	n	0.02 V/Var
$G_{Ic}(s)$ parameters	k_{Ic}, w_{Ic}	15, 400 rad/s
$G_O(s)$ parameters	k_o, w_o	3, 100 rad/s

The MG operates under grid-connected mode. CB is opened at time $t=T_1=4.4$ s consequent to an unintentional islanding

disturbance. After 100 ms, i.e., the time period required for islanding detection algorithm, the MG will go to islanding mode. For the experimental studies, a passive islanding detection approach [30] with criteria of ±10% magnitude voltage deviation and ±0.5Hz frequency deviation is employed.

In GC mode, all the DERs operate in grid-following strategy and are responsible for injecting 300 W to the grid.

Fig. 16 to Fig. 21 show the experimental results of the conventional and the proposed controller during the transition from GC to IS mode. Due to low inertia and lack of enough damping, the output current has a large fluctuation with high overshoot and settling time as shown in Fig. 16(a). By providing more inertia and damping using the proposed controller, deviation of the output current is significantly suppressed, as it can be observed in Fig. 16(b). Accordingly, it behaves like a first order system.

Fig. 17 and Fig.18 show the voltage waveform and the voltage magnitude at bus 1 that has been suffered under voltage and drops to 100 V approximately. The output voltage drop of DERs is remarkably compensated because of the proper performance of the proposed controller. The restoration process of voltage is improved significantly by the proposed controller.
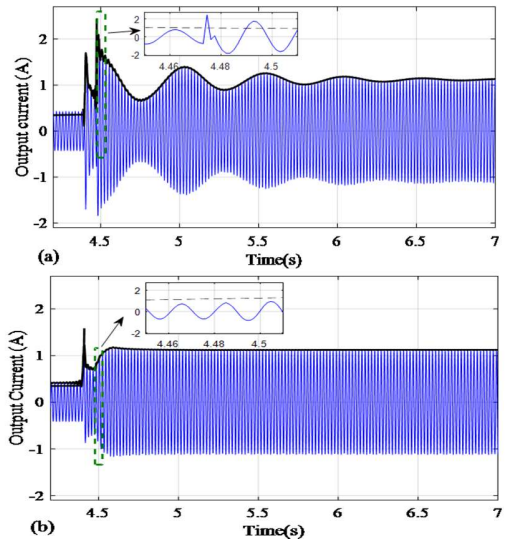

Fig. 16. Output current waveform of DER 1 during transition from grid-connected to islanding mode: (a) conventional strategy, (b) proposed strategy.
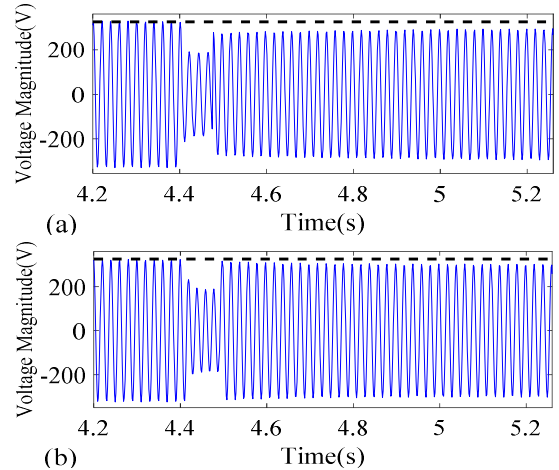

Fig. 17. Output voltage waveforms of DER 1 during transition from grid-connected to islanding mode: (a) conventional strategy, (b) proposed strategy.
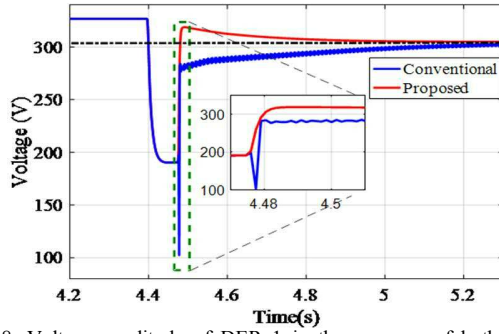
Fig.18. Voltage amplitude of DER 1 in the presence of both conventional strategy and the proposed strategy.

The injected active and reactive power of DER 1 and DER 3 during the transition mode are depicted in Fig. 19 and Fig. 20, respectively. The Large fluctuation in current and voltage results in high oscillatory performance with relatively long duration in active and reactive power of DERs.
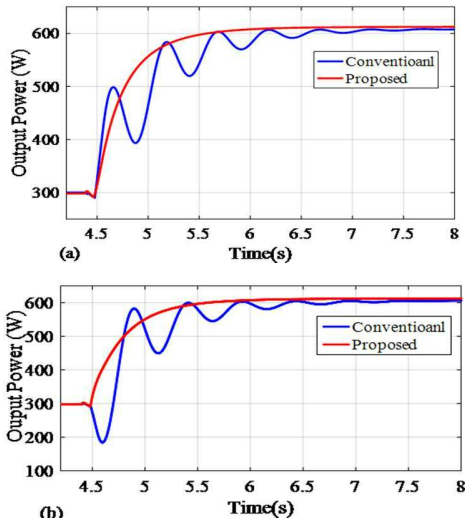

Fig. 19. Generated active power of the DERs in the presence of both controllers, (a) DER 1, (b) DER 3.
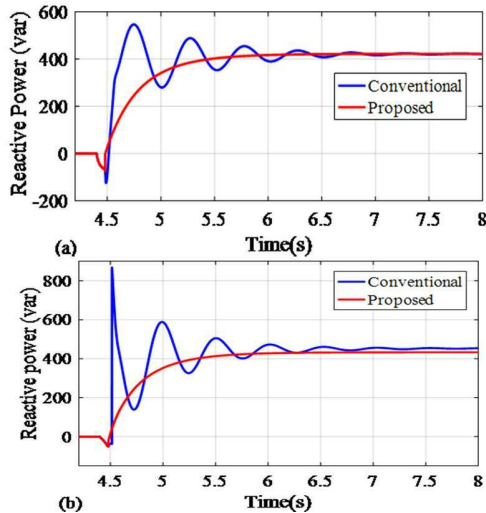

Fig. 20. Generated reactive power of the DERs in the presence of both controllers, (a) DER 1, (b) DER 3.

Since the parallel operation of DERs for active power sharing is based on droop control, and frequency is a function of active power, it has a non-smooth behavior (see Fig. 21). It is obvious that frequency reaches a steady-state value much faster using the proposed controller.
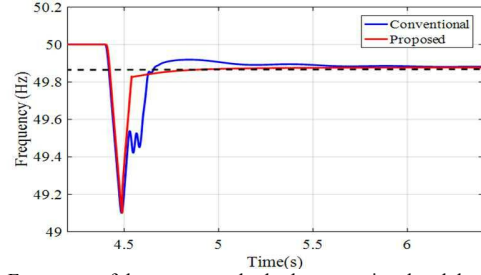

Fig. 21. Frequency of the system under both conventional and the proposed strategy.

The experimental results show that the overshoot of the output current is decreased from 200% in the base case to 5% in the proposed controller. In this case, the settling time of the proposed controller is significantly diminished. Opposed to the conventional approaches, the proposed controller improves the dynamic response, e.g., the overshoot of the voltage magnitude of DER1 is limited to ~15% of the steady-state value.

VI. CONCLUSION

This paper proposes an effective control strategy for smooth transition from grid-connected to islanding mode due to unintentional islanding. The proposed control strategy includes two compensators, i.e., capacitor current feedback, output current feed-forward loops, and a modified droop mechanism. The proposed droop control can reduce the frequency deviation to a desirable level. The performance of the compensator has been analyzed in frequency and time domains. The simulation results show the effectiveness of the proposed controller such as overshoot reduction, bandwidth increasing, and damping improvement. A small signal analysis has been developed for the modified droop control to capture convenient coefficients. To investigate CPL destabilizing effect on the MG, a separate small signal stability with different CPL values have been studied. The theoretical analysis has been verified by the experimental results obtained for both conventional and the proposed control strategy. It has been shown that the proposed control strategy provides a proper performance. Eventually, a smooth transition to islanding mode is guaranteed.

VII. REFERENCES

[1] J. Rocabert, A. Luna, F. Blaabjerg, and P. Rodriguez, "Control of power converters in AC microgrids," *IEEE Trans. Power Electron.*, vol. 27, no. 11, pp. 4734-4749, Nov. 2012.
[2] T. L. Vandoorn, J. C. Vasquez, J. De Kooning, J. M. Guerrero, and L. Vandevelde, "Microgrids: Hierarchical control and an overview of the control and reserve management strategies," *IEEE Ind. Electron. Mag.*, vol. 7, no. 4, pp. 42-55, Dec. 2013.
[3] A. H. Etemadi and R. Iravani, "Supplementary mechanisms for smooth transition between control modes in a microgrid," *Electric Power Systems Research*, vol. 142, pp. 249-257, 2017.
[4] S. Sajadian, and R. Ahmadi, "Model predictive control of dual-mode operations z-source inverter: Islanded and grid-connected," *IEEE Trans. Power Electron.*, vol. 33, no. 5, pp. 4488-4497, May. 2018.

[5] S. M. Ashabani and Y. A.-R. I. Mohamed, "A flexible control strategy for grid-connected and islanded microgrids with enhanced stability using nonlinear microgrid stabilizer," *IEEE Trans. Smart Grid*, vol. 3, no. 3, pp. 1291-1301, Sep. 2012.

[6] J. Kim, J. M. Guerrero, P. Rodriguez, R. Teodorescu, and K. Nam, "Mode adaptive droop control with virtual output impedances for an inverter-based flexible AC microgrid," *IEEE Trans. Power Electron.*, vol. 26, no. 3, pp. 689-701, Mar. 2011.

[7] J. Wang, N. C. P. Chang, X. Feng, and A. Monti, "Design of a generalized control algorithm for parallel inverters for smooth microgrid transition operation," *IEEE Trans. Ind. Electron.*, vol. 62, no. 8, pp. 4900-4914, Aug. 2015.

[8] Y. A.-R. I. Mohamed and A. A. Radwan, "Hierarchical control system for robust microgrid operation and seamless mode transfer in active distribution systems," *IEEE Trans. Smart Grid,* vol. 2, no. 2, pp. 352-362, June. 2011.

[9] X. Li, H. Zhang, M. B. Shadmand, and R. Balog, "Model Predictive Control of Voltage Source Inverter with Seamless Transition between Islanded and Grid-connected Operations," *IEEE Trans. Ind. Electron.*, vol. 64, no. 10, pp. 7906 - 7918, Oct. 2017.

[10] H. Mahmood and J. Jiang, "A control strategy of a distributed generation unit for seamless transfer between grid connected and islanded modes," *in proc. Industrial Electronics (ISIE),* 2014, pp. 2518-2523.

[11] L. G. Meegahapola, D. Robinson, A. Agalgaonkar, S. Perera, and P. Ciufo, "Microgrids of commercial buildings: Strategies to manage mode transfer from grid connected to islanded mode," *IEEE Trans. Sustainable Energy*, vol. 5, no. 4, pp. 1337-1347, Oct. 2014.

[12] C.-L. Chen, Y. Wang, J.-S. Lai, Y.-S. Lee, and D. Martin, "Design of parallel inverters for smooth mode transfer microgrid applications," *IEEE Trans. Power Electron.*, vol. 25, no. 1, pp. 6-15, Jan. 2010.

[13] Z. Guo, D. Sha, and X. Liao, "Voltage magnitude and frequency control of three-phase voltage source inverter for seamless transfer," *IET Power Electron.*, vol. 7, no. 1, pp. 200-208, Jan. 2014.

[14] J. Kwon, S. Yoon, and S. Choi, "Indirect current control for seamless transfer of three-phase utility interactive inverters," *IEEE Trans. Power Electron.*, vol. 27, no. 2, pp. 773-781, Feb. 2012.

[15] G. G. Talapur, H. Suryawanshi, L. Xu, and A. Shitole, "A Reliable Micro-grid with Seamless Transition between Grid Connected and Islanded Mode for Residential Community with Enhanced Power Quality," *IEEE Trans. Ind. Appl.*, vol. 54, no. 5, pp. 5246-5255, Oct. 2018.

[16] J. C. Vasquez, J. M. Guerrero, A. Luna, P. Rodríguez, and R. Teodorescu, "Adaptive droop control applied to voltage-source inverters operating in grid-connected and islanded modes," *IEEE Trans. Ind. Electron.*, vol. 56, no. 10, pp. 4088-4096, Oct. 2009.

[17] Y. Chen, J. M. Guerrero, Z. Shuai, Z. Chen, L. Zhou, and A. Luo, "Fast reactive power sharing, circulating current and resonance suppression for parallel inverters using resistive-capacitive output impedance," *IEEE Trans. Power Electron.,* vol. 31, no. 8, pp. 5524-5537, Aug. 2016.

[18] *IEEE Standard for Interconnecting Distributed Resources with Electric Power Systems*, IEEE Standard 1547, 2003.

[19] G. Lou, W. Gu, J. Wang, J. Wang, and B. Gu, "A unified control scheme based on a disturbance observer for seamless transition operation of inverter-interfaced distributed generation," *IEEE Trans. Smart Grid*, vol. 9, no. 5, pp. 5444-5454, Sep. 2018.

[20] J. Liu, Y. Miura, and T. Ise, "Comparison of dynamic characteristics between virtual synchronous generator and droop control in inverter-based distributed generators," *IEEE Trans. Power Electron.,* vol. 31, no. 5, pp. 3600-3611, May. 2015.

[21] U. Tamrakar, D. Shrestha, M. Maharjan, B. Bhattarai, T. Hansen, and R. Tonkoski, "Virtual inertia: Current trends and future directions," *Applied Sciences,* vol. 7, no. 7, p. 654, June. 2017.

[22] X. Meng, Z. Liu, J. Liu, T. Wu, S. Wang, and B. Liu, "Comparison between virtual synchronous generator and droop controlled inverter," *IEEE 2nd Annual Southern Power Electronics Conference (SPEC)*, pp. 1-6, 2016.

[23] G. Shen, D. Xu, L. Cao, and X. Zhu, "An improved control strategy for grid-connected voltage source inverters with an LCL filter," *IEEE Trans. Power Electron.*, vol. 23, no. 4, pp. 1899-1906, July. 2008.

[24] G. Shen, X. Zhu, J. Zhang, and D. Xu, "A new feedback method for PR current control of LCL-filter-based grid-connected inverter," *IEEE Trans. Ind. Electron.*, vol. 57, no. 6, pp. 2033-2041, June. 2010.

[25] F. D. Freijedo et al., "Tuning of synchronous-frame PI current controllers in grid-connected converters operating at a low sampling rate by MIMO root locus," *IEEE Trans. Ind. Electron*, vol. 62, no. 8, pp. 5006-5017, Aug. 2015.

[26] N. L. Díaz, E. A. Coelho, J. C. Vásquez, and J. M. Guerrero, "Stability analysis for isolated ac microgrids based on pv-active generators," *in proc. Energy Conversion Congress and Exposition (ECCE), 2015,* pp. 4214-4221.

[27] H. Zhang, S. Kim, Q. Sun, and J. Zhou, "Distributed adaptive virtual impedance control for accurate reactive power sharing based on consensus control in microgrids," *IEEE Trans. Smart Grid,* vol. 8, no. 4, pp. 1749-1761, July. 2017.

[28] N. Bottrell, M. Prodanovic, and T. C. Green, "Dynamic stability of a microgrid with an active load," *IEEE Trans. Power Electron.,* vol. 28, no. 11, pp. 5107-5119, Nov. 2013.

[29] N. Pogaku, M. Prodanovic, and T. C. Green, "Modeling, analysis and testing of autonomous operation of an inverter-based microgrid," *IEEE Trans. Power Electron.,* vol. 22, no. 2, pp. 613-625, March. 2007.

[30] W. Bower and M. Ropp, "Evaluation of islanding detection methods for photovoltaic utilityinteractive power systems," *IEA PVPS,* March. 2002.